Astron. Astrophys. 336, L9–L12 (1998)

ASTRONOMY AND ASTROPHYSICS

LETTER

Letter to the Editor

ISO deep far-infrared survey in the "Lockman Hole"

A search for obscured objects at high redshift. I. Observations

K. Kawara[1,2,3], Y. Sato[2,3,4], H. Matsuhara[2,5], Y. Taniguchi[4], H. Okuda[2], Y. Sofue[1], T. Matsumoto[2], K. Wakamatsu[6], H. Karoji[7], S. Okamura[8], K.C. Chambers[9], L.L. Cowie[9], R.D. Joseph[9], and D.B. Sanders[9,⋆,⋆⋆]

[1] Institute of Astronomy, The University of Tokyo, 2-21-1 Osawa Mitaka, Tokyo, 181, Japan
[2] Institute of Space and Astronautical Science (ISAS), 3-1-1 Yoshinodai, Sagamihara, Kanagawa, 229, Japan
[3] ISO Science Operations Centre, Astrophysics Division of ESA, Villafranca, E-28080 Madrid, Spain
[4] Astronomical Institute, Tohoku University, Aoba, Sendai 980-77, Japan
[5] Department of Astrophysics, School of Science, Nagoya University, Furo-cho, Chikusa-ku, Nagoya 464-01, Japan
[6] Department of Physics, Gifu University, Gifu 501-11, Japan
[7] National Astronomical Observatory, 2-21-1 Osawa Mitaka, Tokyo 181, Japan
[8] Department of Astronomy, School of Science, University of Tokyo, Bunkyo-ku, Tokyo 113, Japan
[9] Institute for Astronomy, University of Hawaii, 2680 Woodlawn Drive, Honolulu, HI 96822, USA

Received 2 March 1998 / Accepted 22 May 1998

Abstract. Two $44' \times 44'$ fields in the Lockman Hole were mapped at 95 μm and 175 μm using ISOPHOT. A simple program code combined with PIA works well to correct for drift in the detector responsivity. The number density of 175 μm sources is 3–10 times higher than expected from the no-evolution model.

Key words: galaxies: evolution – galaxies: starburst – cosmology: observations – infrared: galaxies

1. Introduction

As part of the Japan/UH cosmology program using the ISAS guaranteed time, a 95 μm and 175 μm survey was conducted in the Lockman Hole to search for obscured infrared galaxies at high redshift. The very preliminary results and discussion were presented by Kawara et al. (1997a,b). This paper presents observations, image processing, and discussion on the nature of far-infrared sources. Point source extraction from the maps and source counts will be presented in the forthcoming paper (Kawara et al. 1998).

Send offprint requests to: K. Kawara
(kkawara@mtk.ioa.s.u-tokyo.ac.jp)

⋆ Based on observations with ISO, an ESA project with instruments funded by ESA member states (especially the PI countries: France, Germany, the Netherlands, and the United Kingdom) and with the participation of ISAS and NASA.

⋆⋆ The ISOPHOT data presented in this paper was reduced using PIA, which is a joint development by the ESA Astrophysics Division and the ISOPHOT consortium led by the Max Plank Institute for Astronomy (MPIA), Heidelberg.

Table 1. Detectors and filters[a]

Filter	λ_0 (μm)	$\Delta\lambda$ (μm)	Detector array[b]	Array size[c]	Airy diameter[d]
C_90	95.1	51.4	C100	138″	80″
C_160	174.0	89.4	C200	184″	146″

[a] Cited from Klaas et al.(1994)
[b] C100 is a 3×3 Ge:Ga detector array, and C200 a 2×2 stressed Ge:Ga array
[c] The size of each detector pixel is $43.5'' \times 43.5''$ for C100 and $89.4'' \times 89.4''$ for C200, so there are very small gaps between the individual detector pixels.
[d] The FWHM of the Airy disk is $0.422\times$ (the Airy diameter): 34″for C100 and 62″for C200.

2. Observations

We have carried out a far-infrared survey by using ISOPHOT(Lemke et al. 1996) which is an imaging photopolarimeter on board the Infrared Space Observatory (ISO; Kessler et al. 1996). Two fields named LHEX and LHNW, each extending approximately $44' \times 44'$, were selected in the "Lockman Hole", a region of the smallest HI column density in the sky (Lockman et al. 1986), to minimize confusion noise due to infrared cirrus. Table 1 summarizes the combinations of the filters and the detector arrays which were used for the observations.

A pilot observation spending 6.6 hours in total was made in revolution 132 (March 28, 1996) in the PHT32 oversampled maps and scans mode (Klaas et al.1994). A quick data analysis showed that the signals were dominated by electronic noise

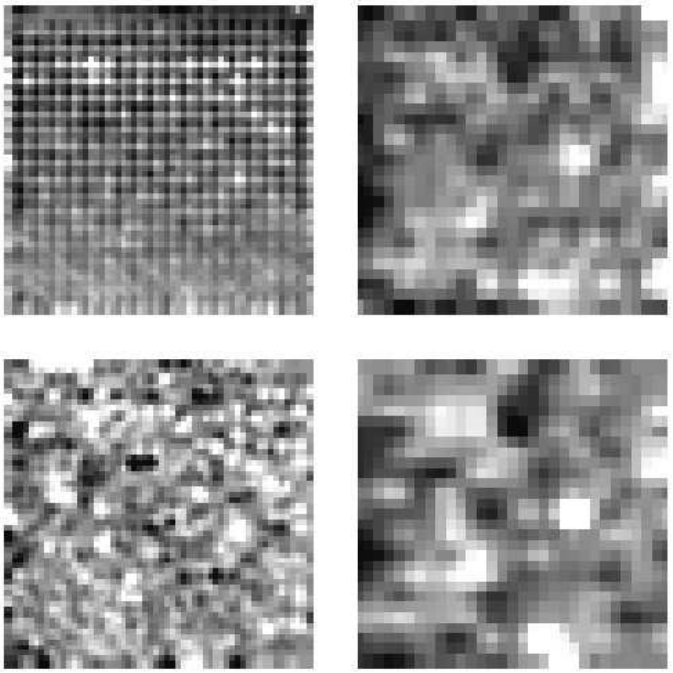

Fig. 1. C_90 and C_160 maps in $22' \times 22'$ sub-field LHEX3. The top panel shows the AAP maps. The C_90 map is on the left and C_160 on the right. The pixel size for the map is $23'' \times 23''$ for C_90 and $46'' \times 46''$ for C_160. The bottom panel shows the maps after our drift correction processing was applied to the AAP maps.

Table 2. PHT22 parameters for mapping a single sub-field

Filter	Raster points	Raster step[a]	Int. ramps per raster point	Background COBE[b]
C_90	18×18	$69''$, $69''$	8 (2 sec / ramp)[c]	4.08
C_160	27×14	$46''$, $92''$	5 (4 sec / ramp)[d]	2.72

[a] $69''$ corresponds to half of the C100 array ($1.5 \times$ one detector pixel), $46''$ to quarter of the C200 array (half of one detector pixel), and $92''$ to half of the array (one detector pixel).
[b] Kindly provided by Reach (1996) in units of (MJy sr^{-1})
[c] The duration of each integration ramp is 2 sec, and the number of non-destructive readouts is 63 per ramp. The integration time per raster point is 16 sec.
[d] The duration of each integration ramp is 4 sec, and the number of non-destructive readouts is 127 per ramp. The integration time per raster point is 20 sec.

due to the short integration ramp containing only three non-destructive readouts. We therefore selected the PHT22 staring raster map mode for the main observations using 35.4 hours, which were executed between revolutions 194 and 215 (May 28 and June 19, 1996). Each of the two fields is made up of four sub-fields having an approximately $22' \times 22'$ area each. Table 2 shows the parameters used for raster mapping of a single sub-field, together with details of the readout settings.

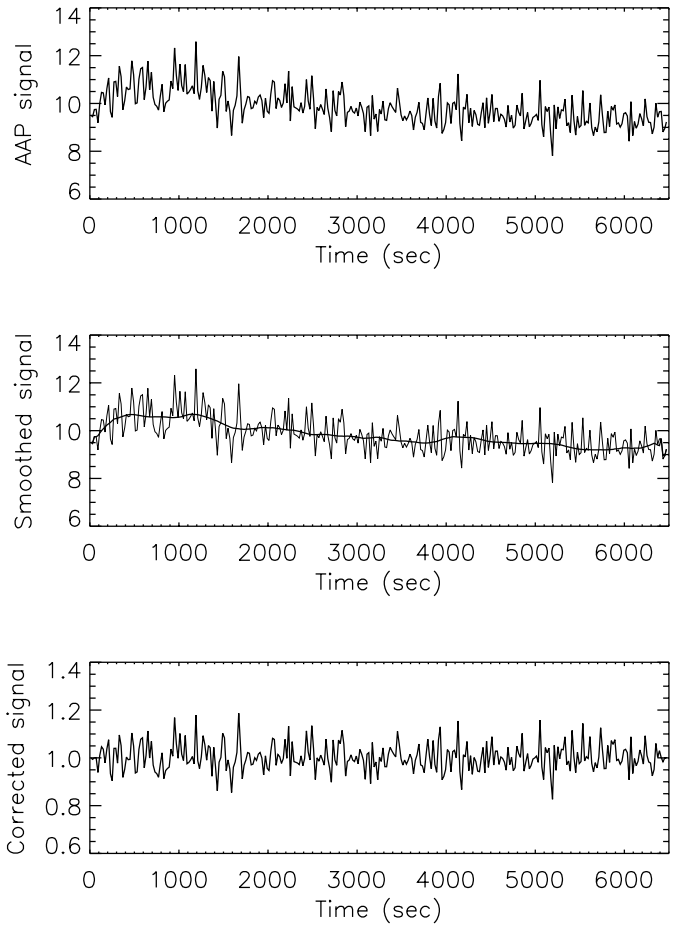

Fig. 2. Signals from C100 detector #5 as a function of time during observing LHEX3. The top panel shows the AAP signal containing high and low frequency fluctuations. The middle panel shows the smoothed signal (thick line) compared with the AAP signal (thin line). The bottom panel shows the drift corrected signal.

3. Image processing

The PHT Interactive Analysis (PIA) version 6.4 was used with the default settings to reduce the edited raw data created in November, 1996 via the off-line processing version 5.1 or 5.2. The top panel in Fig. 1 shows the results (hereafter called AAP map or signal) obtained from the PIA's Astronomical Analysis Processing (AAP). Checked patterns are evident in the C_90 AAP map. This is caused by drift in the responsivity of C100 detectors and unstable characteristics of the internal calibrators.

The top panel of Fig. 2 plots the AAP signal from C100 detector #5 as a function of time; each data point is a median mean of all the integration ramps taken at the respective raster point. This is one dimensional display of 18×18 raster points. The AAP signal consists of high and low frequency fluctuations. The middle panel shows the smoothed signal obtained by filtering off the high frequency fluctuations from the AAP signal. For this filter, IDL's MEDIAN was first applied with WIDTH $\sim 1.5\times$ M. M is the number of raster points along the raster leg (i.e., 18 for C_90 and 27 for C_160 as given in Table 2). To remove small persisting ripples, SMOOTH was then applied

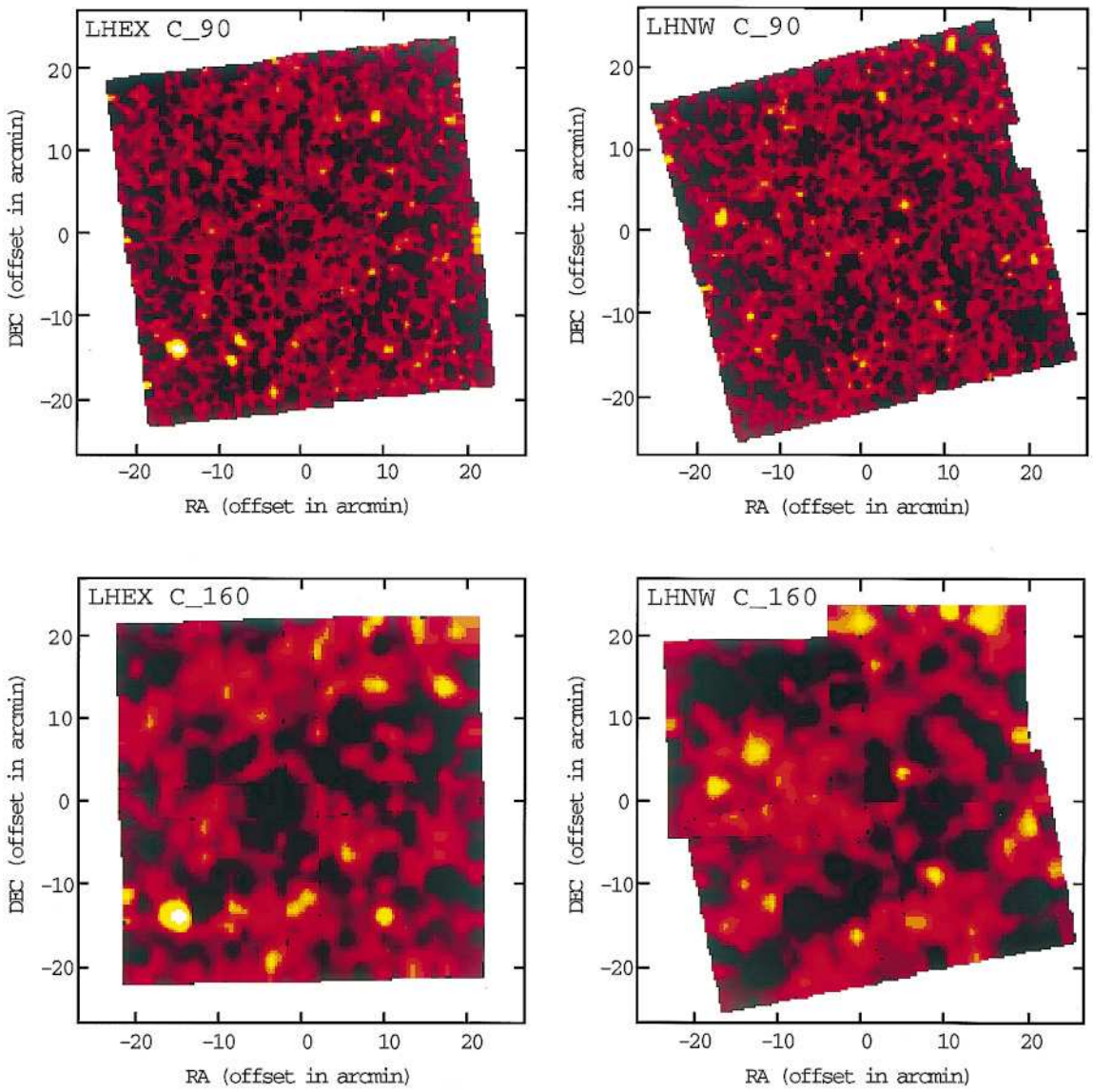

Fig. 3. The left column shows C_90 (top) and C_160 (bottom) maps of $44' \times 44'$ field LHEX at α(J2000) = $10^{\rm h}52^{\rm m}$ and δ(J2000) = 57°, which are made up of four $22' \times 22'$ sub-fields. The drift corrected maps like one as shown in Fig. 1 are rebinned into a scale of $4.6''$/pixel using bi-linear interpolation. The right column shows the same, but for LHNW at α(J2000) = $10^{\rm h}34^{\rm m}$ and δ(J2000) = 58°.

with WIDTH ~ 10. The bottom panel shows the drift corrected signal, which was obtained by dividing the AAP signal by the smoothed signal. This removes the low frequency fluctuations (detector drift) from the AAP signal. The bottom panel of Fig. 1, which was created from the corrected signal, demonstrates the drastic improvement for the C_90 map made by this drift correction processing. The AAP C_160 map is almost identical to that from the corrected signal. Comparison between AAP and corrected C_160 maps shows that the photometric error introduced from this correction is 4% or better and no extended brightness structures recognized within a $22' \times 22'$ area (see Fig. 1 in Kawara et al. 1997a) are affected. Fig. 3 shows the mosaiced maps of LHEX and LHNW, which are made from the corrected signal.

4. Discussion

The flux calibration can be made using either the COBE background measurements listed in Table 2 or the IRAS point source fluxes. Note that the intensity of interplanetary dust emission varies little at such high ecliptic latitude ($\beta \sim 45°$) as the solar elongation changes. The fields contain only one IRAS source (F10507+5723). This is the brightest source detected in our survey and identified with a Sb galaxy UGC 06009 (Thuan & Sauvage 1992). The IRAS fluxes are 533 mJy at 60 μm and 1218 mJy at 100 μm (IRAS FSC 1990). Its flux ratio f(100 μm)/f(60 μm) = 2.29 is fitted to a combination of the infrared cirrus and starburst spectra given by Pearson & Rowan-Robinson (1996), if 76% of the 100 μm flux comes from the cirrus component. This predicts f(175 μm) = 1133 mJy from

f(175 μm)/f(100 μm) = 0.93 which is comparable to that in the inner arm of a Sc galaxy M101 (Hippelein et al. 1996). The COBE based scaling yields 347 mJy at 95 μm and 451 mJy at 175 μm, implying that the COBE based scaling may underestimate point source fluxes by 3.5 at 95 μm and 2.5 at 175 μm. The origin of these differences is unclear. In the following discussion, the ISO fluxes are scaled based on the IRAS measurements.

The maps in Fig. 3 contain numerous spots. Bright spots cannot be attributed to peaks of the infrared cirrus. The total HI column density N_H in our fields is approximately 6×10^{19} cm^{-2} (Jahoda et al. 1990). The correlation between N_H and the infrared cirrus brightness indicates B_{cirrus}(95 μm) = 0.41 MJy sr^{-1}and B_{cirrus}(175 μm) = 0.81 MJy sr^{-1}(Table 2 in Boulanger et al. 1996). Using the models by Gautier et al. (1992) with $\alpha = -2.9$ for the index of the spatial power spectrum of the infrared cirrus, σ_{cirrus}(95 μm) $\sim$ 0.14 mJy and σ_{cirrus}(175 μm) $\sim$ 1.7 mJy are obtained for one sigma cirrus confusion noise. The 3 σ flux levels reached in our survey are tentatively estimated to be $\sim 45 \pm 20$ mJy at 95 μm and $\sim 45 \pm 25$ mJy at 175 μm. Hence, a probability of having a cirrus peak brighter than the detection limits is so low that most of spots are likely to be galaxies.

In the two fields LHEX and LHNW, covering 1.1 square degrees in total, there are 36 and 45 sources brighter than 150 mJy at 95 and 175 μm, respectively. Out of 45 175 μm sources, 36 sources are within the area which was observed at the both wavelength. 31 of the 36 sources have the 95 μm counterparts within 40$''$ that were detected above the 3 σ flux level. The completeness down to 150 mJy is estimated to be almost 100%, because of the low probability of cirrus confusion and the high SNR (signal to noise ratios) detection (typical SNR $\sim$ 10). The cumulative counts down to 150 mJy are thus 1.1×10^5 sources sr^{-1} at 95 μm and 1.3×10^5 sources sr^{-1} at 175 μm. The number density of 175 μm sources brighter than 150 mJy are ten times higher than that expected from the no-evolution model by Guiderdoni et al. (1997, 1998). When the COBE based scaling applies, the 175 μm source density down to 60 mJy (i.e., 150/2.5 = 60) is three times higher than the no-evolution model.

Acknowledgements. The authors wish to thank Rene Laureijs, Carlos Gabriel, Julian Sternberg, and Kazuhiro Shimasaku for their extremely useful discussion. The referee, Michael Rowan-Robinson, made valuable suggestions that substantially improved the presentation of this work.

References

Boulanger, F., Abergel, A., Bernard, J.-P., et al. 1996, A&A 312, 256.
Gautier, T.N., Boulanger, F., P, Pérault, M., & Puget, J.L., 1992, AJ, 103, 1313.
Guiderdoni, B., Bouchet, F.R., Puget, J.-L., Guilaine, G., & Hivon, E., Nature, 390, 257.
Guiderdoni, B., Hivon, E., Bouchet, F.R., & Maffei, B., MNRAS, 295, 877.
Hippelein, H., Lemke, D., Haas, M., et al., 1996, A&A, 315, L82.
IRAS FSC, version 2.0, 1990, Joint IRAS Science Working Group, U.S. Government Printing Office, Washington D.C.
Jahoda, K., Lockman, F.J., & McCammon, D., 1990, ApJ, 354, 184.
Kawara, K., Taniguchi, Y., Sato, S., et al., 1997a, ASP Conf. Ser., 124, 386.
Kawara, K., Taniguchi, Y., Sato, S., et al., 1997b, Proc. of the ESA Symposium, ESA SP-401, p285.
Kawara, K. et al. 1998, in preparation.
Kessler, M.F., Steinz, J.A, Anderegg, M.E., et al., 1996, A&A 315, L27.
Klaas, U., Krüger, H., Heinrichsen, I., Heske, A., & Laureijis, R., 1994, $ISOPHOT\ Observer's\ Manual$, Version 3.1.
Lemke, D., Klaas, U., Abolins, J., et al., 1996, A&A 315, L64.
Lockman, F.J., Jahoda, K., & McCammon, D., 1986, ApJ, 302, 432.
Pearson, C. & Rowan-Robinson, M., 1996, MNRAS, 283, 174.
Reach, W.T., 1996, private communication.
Thuan, T.X.., & Sauvage, M., 1992, A&AS, 92, 749.